Elastic Scattering of Alpha Particles by Intermediate-Mass Nuclei*

B. FERNANDEZ† AND J. S. BLAIR
Department of Physics, University of Washington, Seattle, Washington 98105
(Received 13 October 1969)

Angular distributions of 42-MeV α particles, elastically scattered from ^{40,42,44,48}Ca, ^{46,48,50}Ti, ^{52}Cr, ^{54,56}Fe, ^{58,60,62}Ni have been measured in the forward region with an absolute accuracy of $\pm 0.1°$; in particular, the locations of the minima near 35° (c.m. system) have been determined to within $\pm 0.1°$. The theoretical analysis has been done in three ways, using (a) the Fraunhofer model, (b) a direct parametrization of the scattering amplitude in terms of three parameters, and (c) a standard four-parameter optical model. Strong-absorption radii have been deduced from the critical angular momenta extracted from the scattering amplitudes. In addition, attempts have been made to determine, for the optical-model analysis, other sorts of strong-absorption radii that are more characteristic of the scattering than the usual midpoint radius of the potential. Our analyses indicate that the rate of increase of almost all such strong-absorption radii is smaller within the Ca and Ti isotopes than within the Fe and Ni isotopes, the radius of ^{48}Ca being anomalously small for all types of analysis.

I. INTRODUCTION

IT is well known that the elastic scattering cross sections of medium energy α particles on intermediate-mass nuclei display sharply defined diffraction oscillations and that the locations of the minima of these oscillations almost immediately determine the values of the Fraunhofer "strong-absorption" radii. In the present experiment, elastic scattering of α particles with an incident energy near 42 MeV has been investigated for many of the stable isotopes from ^{40}Ca through ^{62}Ni in order to study the isotopic dependence of several varieties of strong-absorption radii.

The present study has been motivated in part by careful measurements of electron scattering,[1–3] mumesic x-ray spectra,[4–6] and Coulomb displacement energies,[7] which have revealed some surprising features of electric-charge distributions of the Ca and Ti isotopes, and by previous measurements of α-particle scattering in this laboratory[8] and elsewhere.[9,10] The elastic scattering angular distributions of 30.5-MeV α particles[9] have indicated that the strong-absorption radius for ^{44}Ca exceeds that for ^{40}Ca; more recently the elastic scattering from ^{40}Ca and ^{48}Ca has been reinvestigated by this group.[10] Also, as a concomitant to his study of inelastic scattering of 42-MeV α particles by nuclei ranging from ^{40}Ca to ^{54}Fe, Peterson[8] analyzed the elastic scattering cross sections and found a strong indication that the rate of increase of strong-absorption radii of the Ca isotopes was less than the general trend through the Periodic Table. These experiments, however, had not been explicitly designed to point up the anticipated small differences in the cross sections of neighboring nuclei. The available data points in regions of sharp minima were neither plentiful enough nor of high enough accuracy to locate the minima to better than $\pm 0.5°$. It therefore seemed desirable to repeat (and extend) these measurements, giving special attention to the locations of the minima which occur near 35° (c.m.) and to the accuracy with which the scattering angles and beam energy are determined as well as to their stability.

At the outset, we should emphasize that the canonical analyses (and subsequent interpretation) of elastic-α-particle measurements rest on less secure foundations than do the analyses of analogous electromagnetic experiments. In the latter case, a relatively unambiguous chain of argument leads one from the measured cross sections to a charge-density function. In contrast, the only statement that can be made with assurance for α-particle scattering is that the scattering amplitude for elastic scattering from a spin-zero target is given by the expression

$$f(\theta)=\frac{i}{2k}\sum_{l=0}^{\infty}(2l+1)(1-\eta_l)P_l(\cos\theta). \qquad (1)$$

The inversion of this summation to obtain the partial-wave amplitudes η_l, though possible in principle, is rarely carried out in practice in situations which involve many partial waves. Instead, it has become customary to parametrize directly the full-scattering amplitude or

* Work supported in part by the U.S. Atomic Energy Commission.
† On leave from Centre d'Études Nucléaires, Saclay, France.
[1] R. Hofstadter, G. K. Nöldeke, K. J. van Oostrum, L. R. Suelze, M. R. Yearian, B. C. Clark, R. Herman, and D. G. Ravenhall, Phys. Rev. Letters **15,** 758 (1965).
[2] K. J. van Oostrum, R. Hofstadter, G. K. Nöldeke, M. R. Yearian, B. C. Clark, R. Herman, and D. G. Ravenhall, Phys. Rev. Letters **16,** 528 (1966).
[3] H. Thiessen, R. Engfer, and G. J. C. van Niftrik, Phys. Letters **22,** 623 (1966).
[4] J. A. Bjorkland, S. Raboy, C. C. Trail, R. D. Ehrlich, and R. J. Powers, Phys. Rev. **136,** B341 (1964).
[5] R. C. Cohen, S. Devons, A. D. Kanaris, and C. Nissim-Sabat, Phys. Letters **11,** 70 (1964).
[6] R. D. Ehrlich, D. Fryberger, D. A. Jensen, C. Nissim-Sabat, R. J. Powers, V. L. Telegdi, and C. K. Hargrove, Phys. Rev. Letters **18,** 959 (1967).
[7] R. Sherr, B. F. Bayman, E. Rost, M. E. Rickey, and C. G. Hoot, Phys. Rev. **139,** B1272 (1965).
[8] R. J. Peterson, Phys. Rev. **140,** B1479 (1965); see also R. J. Peterson, Ph.D. thesis, University of Washington, 1966 (unpublished).
[9] N. S. Wall, G. Heyman, R. W. Bauer, and A. M. Bernstein, *Congrès International de Physique, II,* edited by P. Gugenbauer (Centre National de la Recherche Scientique, Paris, 1964), p. 866.
[10] A. M. Bernstein, M. Duffy, and E. P. Lippincott, Phys. Letters **30B,** 20 (1969).

the partial-wave amplitudes in terms of simple analytic expressions containing a small number of parameters or to parametrize indirectly the scattering amplitude through a dynamic model, usually the complex optical-potential model. In either procedure, one hopes that a good fit between calculated and observed cross sections means that the parametrized partial-wave amplitudes are close to those of nature. It is an article of faith that fluctuations or resonances in the amplitudes, if present at all, do not alter in any significant way the cross sections and that the parameters of the smoothly varying amplitudes are not spurious. It has been amply demonstrated that this belief is not justified for α particles of lower-energy incident on lighter-[11–14] and intermediate-[15–18] mass targets, where the cross sections, particularly at backward angles, are strongly energy-dependent. However, previous experience does furnish some reason to hope that the forward, if not the backward,[15,17] elastic scattering of 42-MeV α particles by intermediate-mass targets is adequately described by models containing a small number of parameters. As will be seen, a partial study of the energy dependence of the forward angle cross sections does not contradict this assumption.

The present experiments have been analyzed in terms of three models: (1) The crudest of these is the Fraunhofer "black-nucleus" model, for which the only parameter of relevance is a strong-absorption radius. (2) At a somewhat higher degree of sophistication is a three-parameter version of the scattering-amplitudes parametrization introduced by Frahn and Venter.[19] The resulting partial-wave amplitudes are then used to define strong-absorption radii. (3) In addition, calculations have been performed with a standard four-parameter complex optical potential. In view of the well-known ambiguities[20,21] in fixing optical-potential parameters, we have adopted a rather guarded attitude toward the values deduced for these parameters, insofar as they purport to describe the nuclear interior, and instead attach greater significance to the partial-wave amplitudes which emerge from the optical-model analyses. Accordingly, the partial-wave amplitudes and cross sections resulting from the best optical-model fits are used to define strong-absorption radii in a fashion analogous to the recipes used in the scattering-amplitudes parametrization analysis. The significance of these various strong-absorption radii, as well as other sorts of radii characterizing the optical potential in the surface region, is then measured by the extent to which they are consistent with one another, both with respect to absolute magnitudes and to isotopic differences.

II. EXPERIMENTAL ARRANGEMENT AND PROCEDURE

To obtain precise values for the strong-absorption radii, it is necessary that the scattering angles and beam energy have little spread, be stable in time, and be accurately measured. Accordingly, somewhat more care was taken with the experimental arrangement and procedures than is typical of previous α-particle-scattering experiments at this laboratory.

As will be indicated in succeeding sections, we believe that the uncertainty in our mean scattering angles is less than $\pm 0.10°$ and that the median spread about the mean angle is $\pm 0.08°$. The absolute energy of the incident beam could be determined to within ± 0.15 MeV and was always in the neighborhood of 42.0 MeV. More important, the relative energy of the beam could be measured to within ± 50 keV and, during a given run, the beam energy appears to be stable within that value. The uncertainty in energy of degraded beams relative to the undegraded beam is less than ± 0.10 MeV.

To estimate the uncertainties in our determination of radii introduced by the above uncertainties in angle and energy, we were guided by the main result of the diffraction model, namely, that at a given diffraction minimum, the product $2kR\sin(\theta/2)$, or $kR\theta$, equals a constant. According to this criterion, an uncertainty in mean angle of $\pm 0.1°$ at the minima near 35° leads to an uncertainty of $\pm 0.3\%$ in the radius; similarly, an uncertainty of 150 keV in the beam energy results in an uncertainty of $\pm 0.2\%$ in the radius.

A. Angular Accuracy and Angular Spread

The geometry of this experiment is shown in Fig. 1. The incident beam was defined by two collimators $\frac{1}{32}$ in. wide, spaced 20 in. apart except in run IV, where $\frac{1}{16}$-in. collimators were used (see Sec. II F). Targets were placed 8 in. behind the second collimator. For all observations, the foil surfaces were perpendicular to the beam except for the calcium run, where the angle between their normal and the beam direction was 30°. The detector was set 20 in. from the target and was preceded by a $\frac{1}{32}$-in. aperture. In large measure, the tight angular collimation achieved in the present experiment is due to the availability of a 60-in.-diam scattering chamber.

---

[11] T. Mikumo, J. Phys. Soc. Japan **16,** 1066 (1961).
[12] R. A. Atneosen, H. L. Wilson, M. B. Sampson, and D. W. Miller, Phys. Rev. **135,** B660 (1964).
[13] E. B. Carter, G. E. Mitchell, and R. H. Davis, Phys. Rev. **133,** B1421 (1964).
[14] H. J. Kim, Phys. Letters **19,** 296 (1965).
[15] E. T. Boschitz, J. S. Vincent, R. W. Bercaw, and J. R. Priest, Phys. Rev. Letters **13,** 442 (1964).
[16] A. Budzanowski, K. Grotowski, L. Jarczyk, B. Lazarska, S. Micek, H. Niewodniczanski, A. Strzalkowski, and Z. Wrobel, Phys. Letters **16,** 135 (1965).
[17] C. R. Gruhn and N. S. Wall, Nucl. Phys. **81,** 161 (1966).
[18] C. P. Robinson, J. P. Aldridge, J. John, and R. H. Davis, Phys. Rev. **171,** 1241 (1968).
[19] W. E. Frahn and R. H. Venter, Ann. Phys. (N.Y.) **24,** 243 (1963).
[20] G. Igo, Phys. Rev. Letters **1,** 72 (1958).
[21] R. M. Drisko, G. R. Satchler, and R. H. Bassel, Phys. Letters **5,** 347 (1963).

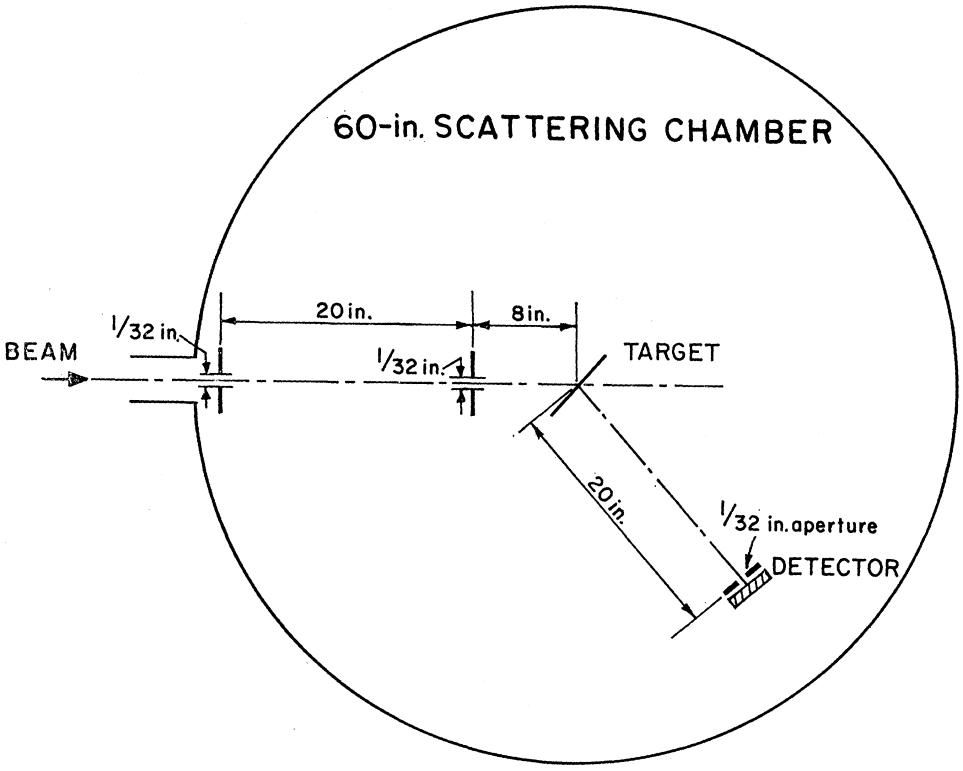

FIG. 1. Geometry of the experiment.

By examining the intensity of the scattered beam for different widths of the incident-beam collimators, we infer that the beam incident on the first collmator is uniformly distributed in position and in incident angle (over the small range of angles permitted by the second collimator). It is then straightforward to calculate the distribution in scattering angles about the mean scattering angle for those particles that are detected. This distribution, whose median spread is $\pm 0.08°$, and whose tail extends to $\pm 0.23°$, takes the form of a diffused trapezoid that drops to half its central value at $\pm 0.12°$. In run IV (see Sec. II F), these values are $\pm 0.11°$, $\pm 0.34°$, and $\pm 0.21°$, respectively.

The contributions to the uncertainty in determining the mean scattering angle are of three sorts: (1) Uncertainties in measuring the detector angle relative to the coordinate system of the scattering chamber. By noting before each run the angular readings corresponding to special fiducial marks in the chamber, we estimate that such uncertainties are less than $\pm 0.02°$. (2) Uncertainties in positioning the target foil (which would imply an uncertainty in location of the origin). Inspection of the target changer and target holders indicates that the uncertainty in mean scattering angle from this source does not exceed $\pm 0.02°$. (3) Uncertainties arising from nonuniformity of the beam incident on the first slit and from nonreproducibility in positioning the collimating slits or mounting the detector. These, as well as those of (1), have been estimated by measuring on both sides of the beam (at the end of each run) the small-angle cross section for elastic scattering of α particles on a thin gold target, normal to the beam. A true zero in mean scattering angle for each run could then be determined to within $\pm 0.05°$. In runs II, III, and IV, the variation in the zeros so determined lies within this same range. In run I, the zero, measured on two separate occasions, differed by $0.17°$ from the mean value found in the other runs. We think that this was due to a slightly different setup, in which the detector was mounted in a different holder on another arm within the chamber. Combining all of these effects, we think that the absolute value of the mean scattering angle can be determined to within $\pm 0.10°$ and that the difference in any two angles during the same run can be specified to within $\pm 0.05°$.

B. Beam Energy

The energy of the incident beam has been measured by a "cross-over" method.[22] Two angles θ_1 and θ_2 were determined such that α particles at θ_1, elastically scattered from a ^{12}C target, have the same final energy as those at θ_2, which have been inelastically scattered

[22] I. M. Naqib and J. S. Blair Phys. Rev. **165**, 1250 (1968).

TABLE I. Target thickness and enrichment.

Nuclide	Thickness $\mu g/cm^2$	Isotope enrichment (%)	Noticeable contaminants
^{40}Ca	600	99.97	
^{42}Ca	750	94.42	4.96% of ^{40}Ca
^{44}Ca	750	98.56	1.35% of ^{40}Ca
^{48}Ca	650	81.9	15.67% of ^{40}Ca, 2% of ^{44}Ca
^{44}Ti	1150	86.1	10.8% of ^{48}Ti, some iodine
^{9}Ti	900	94.4	Some iodine
^{50}Ti	1340	76.4	17.8% of ^{48}Ti, some iodine
^{52}Cr	540	99.9	
^{54}Fe	2900	96.66	2.34% of ^{56}Fe
^{56}Fe	1200	99.9	
^{58}Ni	490	99.9	
^{60}Ni	2900	99.8	
^{62}Ni	3400	>98	
^{40}Ca[a]	2800	96.9	2% of ^{44}Ca

[a] This target was used only for the runs at 40.65 and 39.21 MeV and was made of natural calcium.

from the first 2^+ level in ^{12}C. The accuracy of this method, which depends on the precision to which the difference $(\theta_1-\theta_2)$ can be measured as well as the precision with which the center of a peak can be located in the energy spectrum, is estimated to be ± 0.15 MeV.

After analyses of our data were completed, we became aware that recent redeterminations of the energy of the first 2^+ level[23] give the value 4.440 MeV instead of the traditional value 4.433 MeV. Use of the new value would increase mean energies (listed in Table II) by 65 keV and would typically reduce the values deduced for the various strong-absorption radii by 0.005 F, an amount which is negligible in comparison to other uncertainties inherent to the experiment and its analysis.

In addition to the above absolute energy measurement, possible variations in this energy were monitored repeatedly throughout all runs using a device constructed by Kavaloski.[24] α particles, elastically scattered from a thin gold foil, were degraded to about 9 MeV by an aluminum foil and detected at the 20° side port to the chamber. The energy of these particles was then compared to those of the two α-particle groups at 8.78 and 6.05–6.09 MeV produced by a thorium source. This method indicated that the beam energy during each particular run was steady to within ± 50 keV. From one run to another, the variations never exceeded 0.3 MeV. On the basis of many experiments performed at the cyclotron over the past few years, the incident-beam spread was estimated to be about ± 40 keV.

[23] J. J. Kolata, R. Auble, and A. Galonsky, Phys. Rev. **162**, 957 (1967).
[24] R. E. Brown, J. S. Blair, D. Bodansky, N. Cue, and C. D. Kavaloski, Phys. Rev. **138**, B1394 (1965).

The energy loss in the targets, which ranged in thickness from 0.6 to 3.4 mg/cm², has been taken into account in calculating the mean energy for each target (as listed in Table I).

Experiments were also carried out using an incident beam that had been degraded by beryllium foils placed between the beam-defining slits and the analyzing magnet. The energies of the incident beam after degradation could be measured to an accuracy of ± 0.1 MeV relative to that of the undegraded beam by comparing the energy spectra of α particles scattered from Au and C targets, both with and without degraders. The degraded incident energies used in these experiments were 40.65 and 39.21 MeV.

C. Detection

The particles were detected by 1-mm-thick surface-barrier Li-drifted silicon detectors whose pulses were amplified and analyzed with standard electronic equipment. The counting rate was sufficiently low so that the correction for the dead time in the analog-to-digital converter was always less than 5%.

D. Targets

The properties of the targets are tabulated in Table I. Heavy contaminants presented problems only in isolated cases. Some iodine was found to be present in the titanium spectra at angles larger than 20°. The iodine cross sections were extrapolated to smaller angles by an optical-model calculation. The correction was always less than 5%. The presence of other isotopes of the same element was generally negligible. However, an important correction was necessary for the ^{48}Ca target, which contained about 15% of ^{40}Ca, because the cross sections from these two isotopes were then very different in the minimum.

The lighter surface contaminants, or the elements present in the backing, C and O, were separated from the elastic peak everywhere but at the angles below 15°. At these angles, their contribution to the elastic peak was estimated by measuring both the number of counts due to excited states in C and O and the ratios of ground-state to excited-state peaks in the spectra with C and Mylar targets.

E. Normalization of Cross Sections

Although the relative cross sections at the maxima can be measured to within a few percent, the absolute cross sections can be determined only to within 10 or 15% at best, from purely experimental considerations, because of uncertainties in foil thickness, detector solid angle, and incident-beam current. In contrast, optical-model calculations which yield any reasonable description of the observed diffraction structure show very little variation in magnitude at small angles.

Stated alternatively, theoretical analyses based on erroneous absolute cross sections can lead to rather

untrustworthy parameters.[25,26] A least-squares-fitting procedure applied to erroneous absolute cross sections will not be able to reduce the discrepancies at the forward angles, but it will strain very hard to obtain a fit at larger angles, at the expense of worsening the fit to the accurately measured slope of the envelope passing through the maxima. In view of the stability of the small-angle optical-model calculations and the consequences of erroneous normalization, we have therefore normalized our data at the most forward angles to the optical-model calculations, thinking that the resulting scale for absolute cross sections will be uncertain to no more than 2 or 3%.

F. Procedure

The experiment comprised four separate runs. To emphasize the differences between isotopes, in each run the cross sections for all isotopes were measured at a given detector angle before moving on to another angle. In hindsight, however, we find that such precautions were probably unnecessary since our determinations of scattering angle appeared to be very stable. In all runs, elastic angular distributions were measured in steps of 1° and 2° from 15° to 40° or 50° (c.m.). Particular attention was given to the minimum near 35° (c.m.) and to the minimum near 24° for the calcium isotopes, where smaller step sizes were chosen. For the Ca isotopes, the step size was 0.2° and for other isotopes, it was 0.2°–0.4°. Run I comprised the four Ca isotopes. In run II, the Fe and Ni isotopes were studied. ^{52}Cr and the Ti isotopes were investigated in run III. The energy dependence of the strong-absorption radii was studied in run IV where scattering cross sections from ^{40}Ca, ^{50}Ti, and ^{62}Ni were measured at incident energies of 40.65 and 39.21 MeV. Wider collimators were used in this run because of the beam loss due to the degradation (70% at 40.65 MeV and 90% at 39.21 MeV).

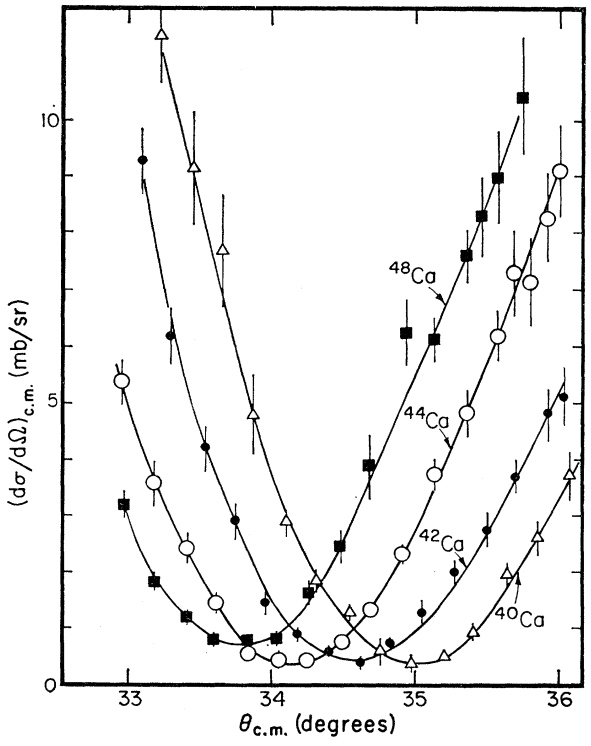

FIG. 2. Observed elastic cross sections in the minima near 35° for run I comprising the Ca targets.

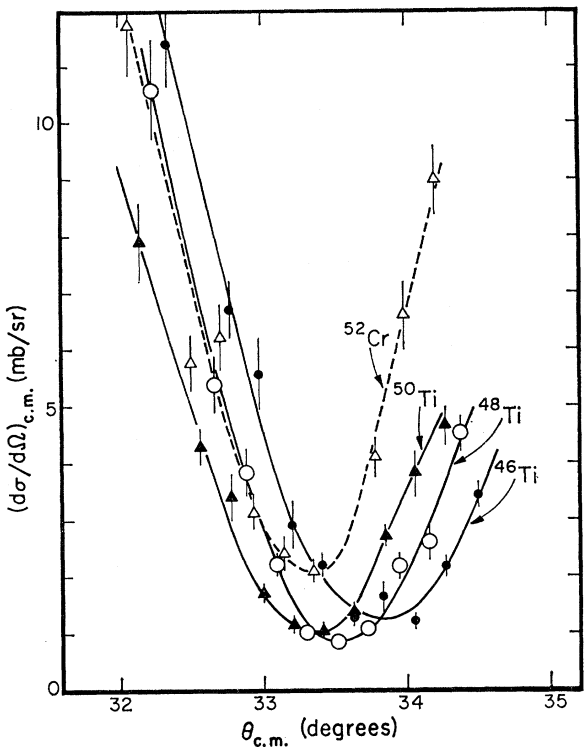

FIG. 3. Observed elastic cross sections in the minima near 34° for run III comprising ^{52}Cr and Ti targets.

III. ANALYSIS

A. Fraunhofer "Black-Nucleus" Model

The only aspect of the Fraunhofer model of which we make use is the statement that minima of the cross sections occur at angles θ_m, for which $J_1(x)=0$, where x is taken to be either $2kR_F \sin(\theta_m/2)$ or $(kR_F\theta_m)$. More specifically, we focus our attention on the minima near 35° (c.m.), and there extract R_F from the requirement that $x=10.173$.

The position of a minimum has been determined not only by observing the angles where the cross sections are smallest, but also, since the former are points with large relative error, from inspection of the sides of the trough around the minimum. By sliding the experi-

[25] J. K. Dickens, Phys. Rev. **143**, 758 (1966).
[26] A. Budzanowski, R. Dymarz, K. Grotowski, and A. Strzalkowski, Institute of Nuclear Physics, Cracow, Report No. 544/P, 1967 (unpublished).

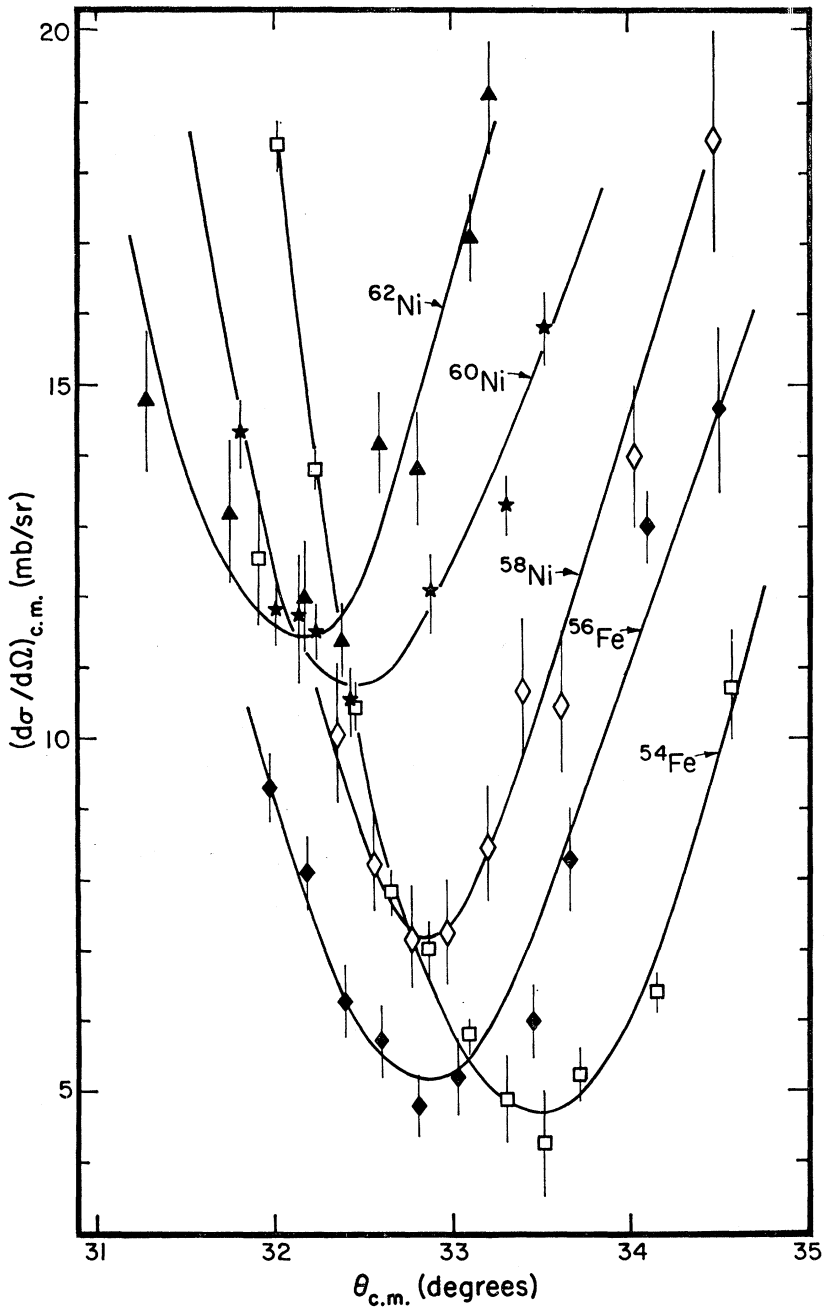

FIG. 4. Observed elastic cross sections in the minima near 33° for run II comprising Fe and Ni isotopes.

mental curves across one another, we visually decided what could be the minimum and the maximum difference in the position of minima for any two isotopes in the same run. The absolute value of θ_m is then determined by an average, using all possible couples of these differences. The error in this graphical procedure is estimated to be $\pm 0.05°$ for runs I and III and perhaps as much as $\pm 0.10°$ for run II.

Figures 2–4 show the behavior of the cross sections at these minima for runs I, III, and II, respectively, and how the minima shift toward smaller angles when the radius increases in a series of isotopes. When the charge is increased, however, the minimum shifts toward a larger angle, reflecting the fact that the Coulomb barrier is higher, thus lowering the critical angular momentum for a grazing collision. The effect of the Coulomb barrier is accounted for explicitly by defining a Coulomb-corrected radius R_{FC} through the expression[19]

$$R_{FC}=ZZ'e^2/2E+[R_F^2+(ZZ'e^2/2E)^2]^{1/2}. \quad (2)$$

(Here Ze is the charge of the target, $Z'e$ is the charge of

the projectile, while E is the energy in the c.m. system.)

The angles where the minimum occurs and the corresponding radii R_{FC} with both choices for the argument x, are listed in Table II. Combining the uncertainties of the analysis and experiment, we estimate that the differences in R_{FC} for isotopes corresponding to a given run can be specified to within ± 0.02 F. Similarly, considering all factors except the uncertainty in absolute energy scale, we estimate that the absolute values of R_{FC} are uncertain to no more than ± 0.03 F.

B. Scattering Amplitudes Parametrization

We have used the following parametrization[19] of the scattering amplitude:

$$\eta_l = g(l) + iA\Delta[dg(l)/dl], \tag{3}$$

where

$$g(l) = \{1 + \exp[(L-l)/\Delta]\}^{-1}. \tag{4}$$

A computer code optimized the three parameters L, Δ, and A in order to minimize the quantity

$$\chi^2 = N^{-1} \sum_{i=1}^{N} \left[\frac{\sigma_{\text{theor}}(\theta_i) - \sigma_{\text{expt}}(\theta_i)}{\Delta\sigma(\theta_i)} \right]^2. \tag{5}$$

Here, N is the number of data points, $\sigma_{\text{theor}}(\theta_i)$ is the theoretical cross section at the angle θ_i, $\sigma_{\text{expt}}(\theta_i)$ is the experimental cross section at θ_i, and $\Delta\sigma(\theta_i)$ the absolute error in $\sigma_{\text{expt}}(\theta_i)$. However, in order to emphasize the location of the minimum near 35°, we have set a uniform error of 1% instead of the actual errors. We did not use the more sophisticated parametrization of Springer and Harvey[27] because the information in these forward-angle angular distributions was too meagre, and this led to large ambiguities, even with a version containing only four parameters.

TABLE II. Fraunhofer analysis.

Nuclide	Energy (Lab) (MeV)	$\theta_{\min}$ (c.m.)	R_{FC} $(2kR\sin(\theta/2))$	R_{FC} $(kR\theta)$
^{40}Ca	41.78	35.00	7.382	7.281
	40.48	35.51	7.421	7.316
	39.03	36.36	7.423	7.314
^{42}Ca	41.76	34.58	7.428	7.329
^{44}Ca	41.76	34.14	7.481	7.383
^{48}Ca	41.77	33.76	7.500	7.404
^{46}Ti	41.92	33.80	7.586	7.490
^{48}Ti	41.94	33.53	7.610	7.515
^{50}Ti	41.92	33.37	7.620	7.526
	40.58	33.97	7.643	7.546
	39.13	34.81	7.642	7.540
^{52}Cr	41.96	33.28	7.695	7.601
^{54}Fe	42.02	33.40	7.729	7.635
^{56}Fe	42.08	32.80	7.821	7.730
^{58}Ni	42.12	32.80	7.883	7.791
^{60}Ni	42.00	32.50	7.939	7.848
^{62}Ni	41.98	32.05	8.017	7.928
	40.45	32.67	8.061	7.967
	39.01	33.54	8.056	7.959

From the scattering amplitudes parametrized in this way, we can define two kinds of critical angular momenta: $L_{p\frac{1}{2}}$ such that $\mathrm{Re}(\eta_{L_{p\frac{1}{2}}}) = \frac{1}{2}$ (which is simply L itself), and $\bar{L}_{p\frac{1}{2}}$, such that

$$T_{\bar{L}_{p\frac{1}{2}}} = 1 - |\eta_{\bar{L}_{p\frac{1}{2}}}|^2 = \tfrac{1}{2}. \tag{6}$$

We can then relate $L_{p\frac{1}{2}}$ and $\bar{L}_{p\frac{1}{2}}$ to strong-absorption radii $R_{p\frac{1}{2}}$ and $\bar{R}_{p\frac{1}{2}}$, respectively, through the definition

$$E = ZZ'e^2/R + (\hbar^2/2mR^2)L(L+1), \tag{7}$$

where m is the reduced mass. Further, we can define a radius $R_{p\sigma}$ in terms of the reaction cross section through the expression

$$E = ZZ'e^2/R_{p\sigma} + (\hbar^2/2mR_{p\sigma}^2)\left[\sum_l (2l+1)T_l\right]. \tag{8}$$

The parameters obtained and the different radii are listed in Table III, and the radii are plotted versus $A^{1/3}$ in Fig. 5. As expected from our definitions, we find that $R_{p\sigma} > \bar{R}_{p\frac{1}{2}} > R_{p\frac{1}{2}}$. The differences $(\bar{R}_{p\frac{1}{2}} - R_{p\frac{1}{2}})$ and $(R_{p\sigma} - R_{p\frac{1}{2}})$ are not constant with changing A, but the three types of radii do show much the same isotopic dependence.

Faivre, Krivine, and Papiau[28] have analyzed the elastic scattering of 44-MeV α particles from a variety of targets, including ^{40}Ca, ^{46,48,50}Ti, ^{52}Cr, ^{54,56}Fe, and ^{58,60,62}Ni, using the parametrization of the scattering amplitudes in terms of five parameters. There are, however, qualitative differences between their resulting strong-absorption radii and our own.

C. Optical Model

We used here the following traditional four-parameter optical potential

$$V_{\text{op}}(r) = (V + iW)\{1 + \exp[(r - R_{\text{opt}})/a]\}^{-1}. \tag{9}$$

A computer code written by one of us (B.F.) optimized the parameters in order to minimize the quantity χ^2 defined in Eq. (5). Again we used uniform weight in order to emphasize the minimum near 35°.

There have been many speculations concerning the appropriate value of V, the depth of the real potential. To determine whether we should favor one value over another, we analyzed a preliminary angular distribution from ^{42}Ca with values of V varying from -40 to -220 MeV in steps of 10 MeV. In the search, V was fixed, and in a first step only W and R_{opt} were allowed to vary. Then, in a second step, W, R_{opt}, and a were allowed to vary. The result of these analyses were the following: (a) Identical angular distributions were obtained for $80 \leq -V \leq 220$. The partial-wave scattering amplitudes rarely changed by more than 0.01. (Thus, these cases yield essentially the same values for strong-

[27] A. Springer and B. G. Harvey, Phys. Letters **14**, 116 (1965).

[28] J. C. Faivre, H. Krivine, and A. M. Papiau, Nucl. Phys. **A108**, 508 (1968).

TABLE III. Analysis of elastic scattering of 42-MeV α particles with scattering-amplitudes parametrization.

Nuclide	Mean energy (Lab) (MeV)	L	Δ	A	$R_{p\frac{1}{2}}$ (F)	$\bar{R}_{p\frac{1}{2}}$ (F)	$R_{p\sigma}$ (F)	χ (%)
^{40}Ca	41.78	16.201	0.772	1.404	7.296	7.450	7.508	34
^{42}Ca	41.76	16.392	0.886	1.280	7.340	7.541	7.604	33
^{44}Ca	41.76	16.599	0.889	1.265	7.390	7.594	7.656	33
^{48}Ca	41.77	16.888	0.910	1.251	7.447	7.657	7.720	25
^{46}Ti	41.92	16.752	0.867	1.283	7.489	7.683	7.744	21
^{48}Ti	41.94	16.876	0.925	1.299	7.509	7.713	7.780	30
^{50}Ti	41.92	17.019	0.861	1.317	7.542	7.728	7.789	22
^{52}Cr	41.96	17.064	0.786	1.412	7.617	7.768	7.826	19
^{54}Fe	42.02	17.022	0.834	1.380	7.659	7.825	7.889	16
^{56}Fe	42.08	17.343	0.897	1.312	7.754	7.945	8.009	21
^{58}Ni	42.12	17.403	0.821	1.438	7.838	7.989	8.051	22
^{60}Ni	42.00	17.610	0.865	1.254	7.911	8.105	8.162	18
^{62}Ni	41.98	17.949	0.873	1.248	8.023	8.220	8.277	14

absorption radii.) (b) The diffuseness a remained essentially unchanged from the value 0.600 F. (c) The ratio V/W remained approximately equal to 3.2. We therefore concluded that V could be chosen arbitrarily and we fixed it to be -200 MeV in all further analyses.

All analyses were then made in three steps: First, only R was allowed to vary, then R and W, and finally R, W, and a. We found that we could not reproduce the cross sections for angles beyond 45° without either sacrificing the quality of the fit to the smaller angles or introducing different radii for the real and imaginary parts of the potential. Accordingly, we decided to concentrate on angles smaller than 45°, which are probably more meaningful for determining a diffraction radius,

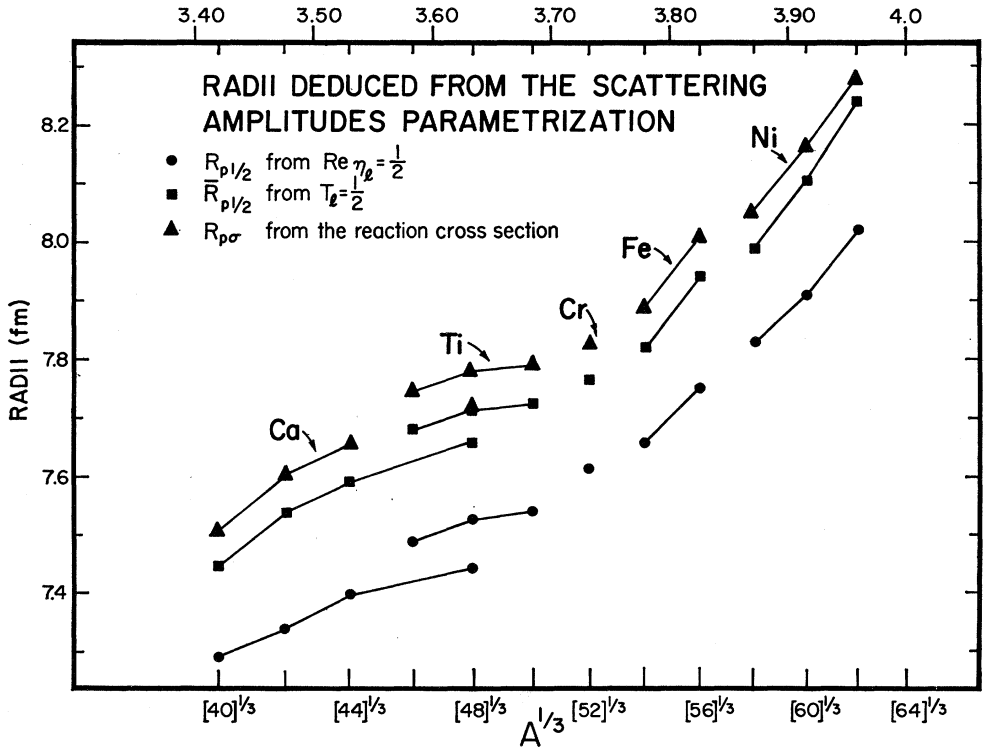

FIG. 5. Strong-absorption radii deduced from the scattering-amplitudes parametrization plotted versus $A^{1/3}$.

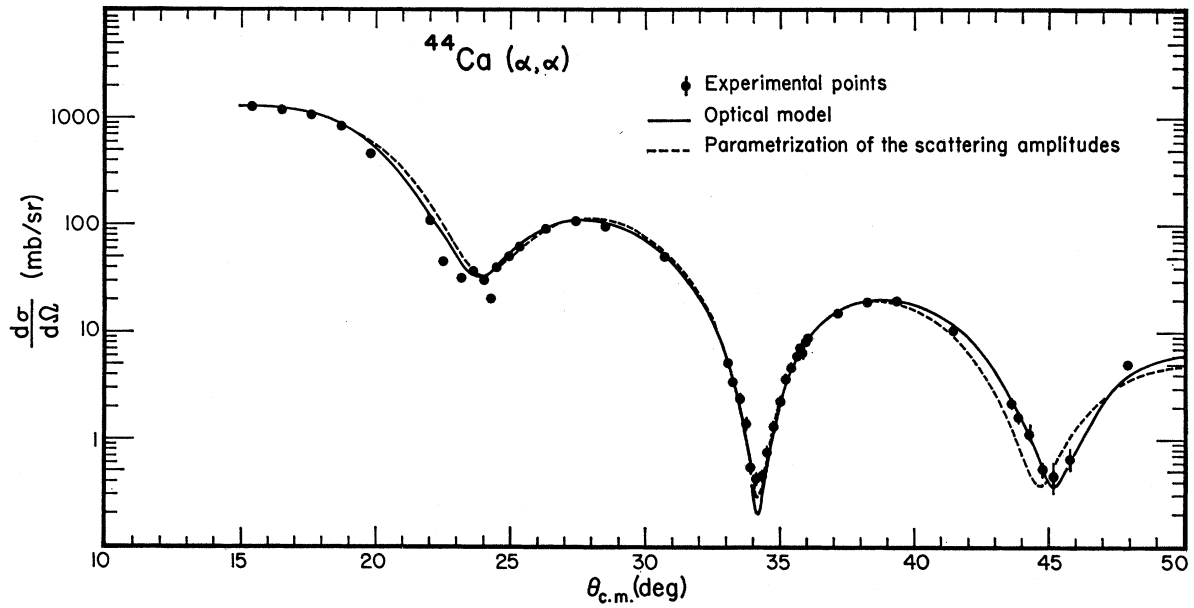

FIG. 6. Experimental c.m. differential cross sections for elastic scattering of 41.76-MeV α particles from ^{44}Ca together with the best-fit cross sections of the optical model and the parametrization of the scattering amplitudes.

rather than on larger angles where the cross sections may be more sensitive to details of the potential.

Strong-absorption radii $R_{\frac{1}{2}}$ and $\bar{R}_{\frac{1}{2}}$ were extracted from the scattering amplitudes in a way very similar to the phenomenological parametrization in Sec. III B. We define $L_{\frac{1}{2}}$ such that $\eta_{L_{\frac{1}{2}}}=\frac{1}{2}$ and $\bar{L}_{\frac{1}{2}}$ such that $T_{\bar{L}_{\frac{1}{2}}}=\frac{1}{2}$. More explicitly, these parameters were obtained from a least-squares fit of the function

$$\eta_l'=\{1+\exp[(L_{\frac{1}{2}}-l)/\delta]\}^{-1} \tag{10}$$

to the scattering amplitudes, and a function

$$T_l'=\{1+\exp[(l-\bar{L}_{\frac{1}{2}})/\bar{\delta}]\}^{-1} \tag{11}$$

to the transmission coefficients in the transition region.

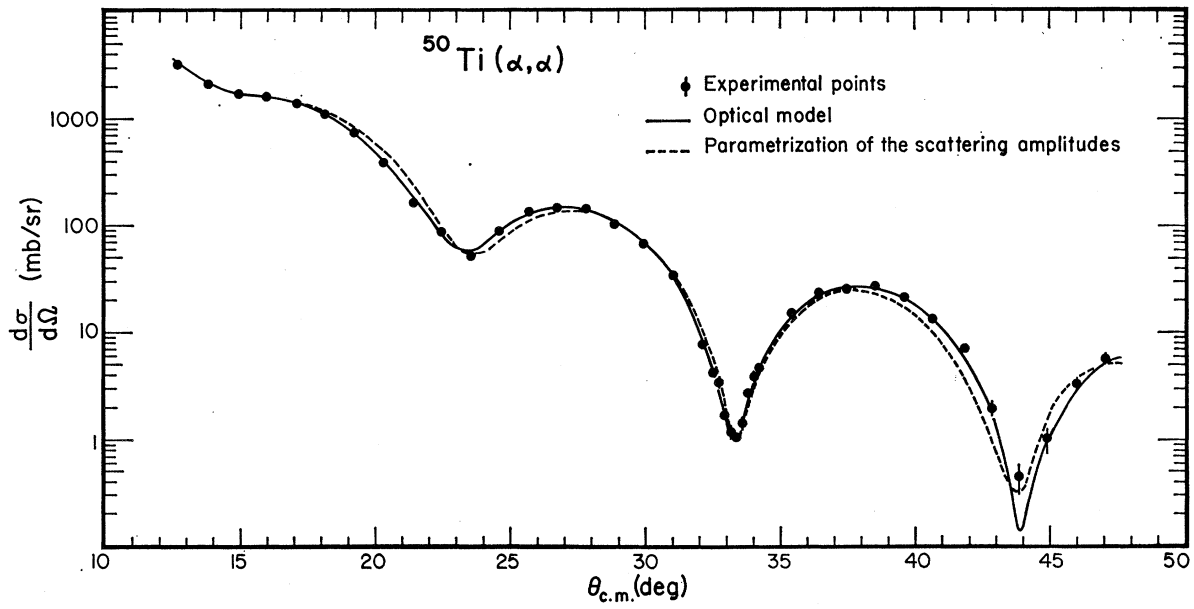

FIG. 7. Experimental c.m. differential cross sections for elastic scattering of 41.92-MeV α particles from ^{50}Ti together with the best-fit cross sections of the optical model and the parametrization of the scattering amplitudes.

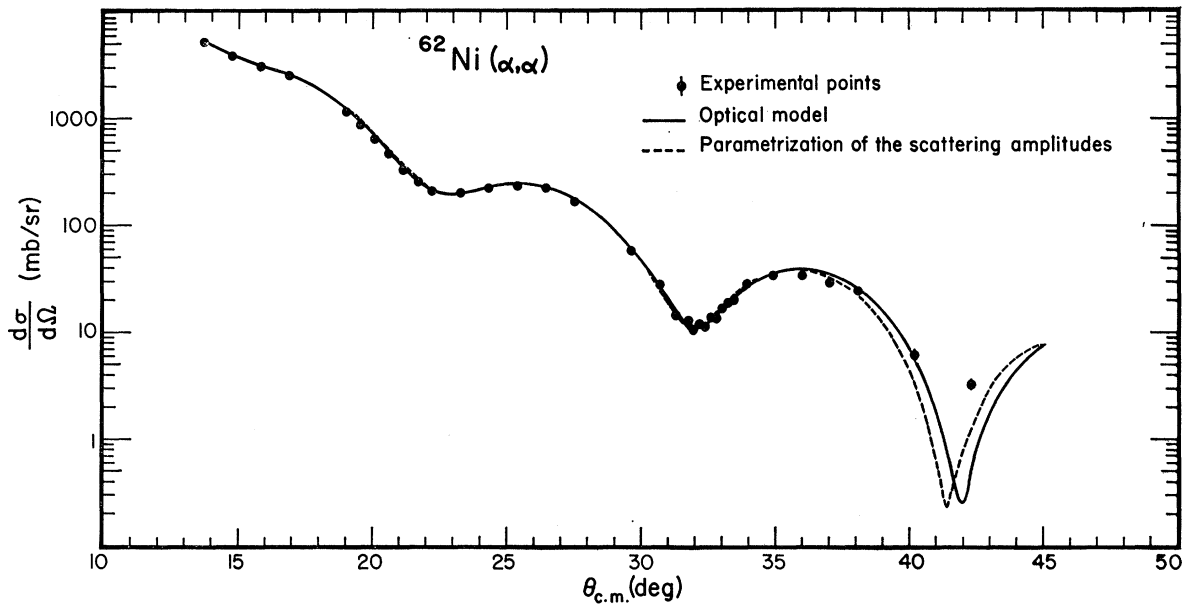

FIG. 8. Experimental c.m. differential cross sections for elastic scattering of 41.98-MeV α particles from ^{62}Ni together with the best-fit cross sections of the optical model and the parametrization of the scattering amplitudes.

In addition, we define a radius R_σ for the optical-model analysis through a formula completely analogous to Eq. (8). All best-fit optical-model parameters are listed in Table III together with the strong absorption radii $R_{\frac{1}{2}}$, $\bar{R}_{\frac{1}{2}}$, and R_σ. Typical angular distributions, with the best theoretical fits for both the scattering-amplitudes parametrization and optical model, are shown in Figs. 6–8.

Calculations have also been performed using a single value for the diffuseness parameter $a=0.573$ F, which is the average of those found in the above analyses. The fits so obtained were nearly as good as those found when the diffuseness parameter was allowed to vary. The differences between $R_{\frac{1}{2}}$ for fixed or freely varying diffuseness are all less than ± 0.006 F, except for the case of ^{52}Cr where the difference is 0.021 F. Further, with the value $a=0.573$ F, it is found that the difference $(R_{\frac{1}{2}}-R_{\rm opt})$ is nearly a constant, 2.523 F$=$ 4.4(0.573) F, for all isotopes; the largest deviations from this result do not exceed ± 0.02 F. Accordingly, for the case of freely varying diffuseness, we have compared $R_{\frac{1}{2}}$ to the sum $(R_{\rm opt}+4.4a)$ and found again that the differences do not exceed ± 0.02 F. This provides us with a useful semiempirical rule for relating $R_{\rm opt}$ and $R_{\frac{1}{2}}$ when, by convention, V is taken to be -200 MeV. The correspondence of $R_{\rm opt}$ to either $\bar{R}_{\frac{1}{2}}$ or R_σ

TABLE IV. Optical-model analysis of elastic scattering of 42-MeV α particles; here $V=-200$ MeV.

Nuclide	Energy (Lab) (MeV)	Optical-model parameters $-W$ (MeV)	$R_{\rm opt}$ (F)	a (F)	R_7 (F)	Strong-absorption radii $R_{\frac{1}{2}}$ (F)	$\bar{R}_{\frac{1}{2}}$ (F)	R_σ (F)	R_b (F)
^{40}Ca	41.78	21.95	4.914	0.554	6.751	7.360	7.461	7.493	7.416
^{42}Ca	41.76	28.42	4.958	0.555	6.799	7.385	7.519	7.564	7.464
^{44}Ca	41.76	40.69	4.927	0.573	6.827	7.429	7.590	7.644	7.493
^{48}Ca	41.77	52.04	4.921	0.586	6.865	7.498	7.662	7.732	7.529
^{46}Ti	41.92	39.90	5.053	0.565	6.927	7.521	7.692	7.743	7.603
^{48}Ti	41.94	43.28	4.999	0.582	6.929	7.566	7.711	7.772	7.603
^{50}Ti	41.92	38.39	5.078	0.569	6.965	7.586	7.729	7.782	7.640
^{52}Cr	41.96	26.29	5.274	0.539	7.062	7.645	7.795	7.829	7.747
^{54}Fe	42.02	32.46	5.208	0.562	7.072	7.693	7.833	7.877	7.764
^{56}Fe	42.08	44.60	5.166	0.588	7.116	7.762	7.915	7.981	7.810
^{58}Ni	42.12	27.86	5.324	0.566	7.201	7.826	7.964	8.004	7.905
^{60}Ni	42.00	42.97	5.367	0.572	7.264	7.897	8.075	8.127	7.974
^{62}Ni	41.98	54.30	5.370	0.595	7.343	8.001	8.196	8.265	8.060

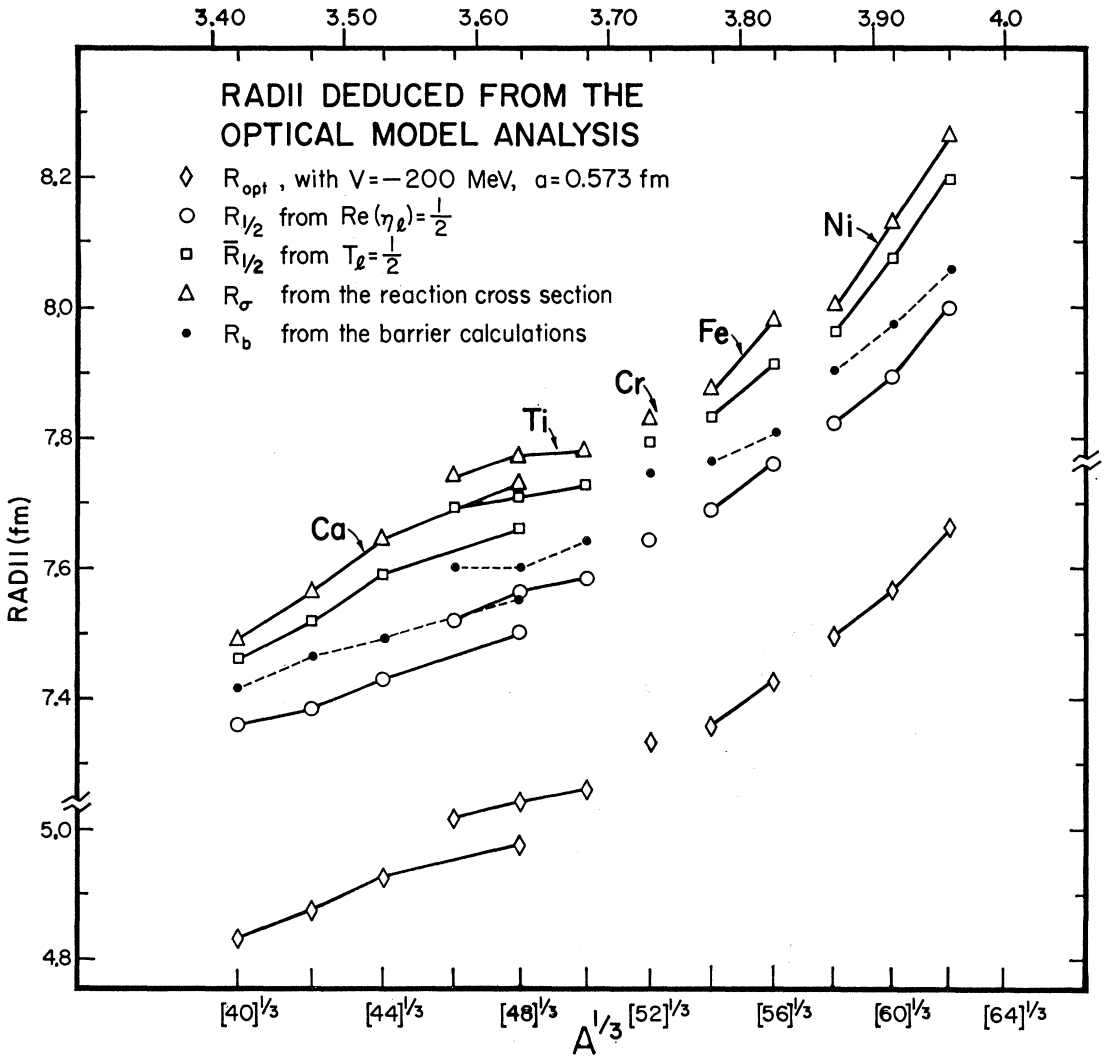

FIG. 9. Strong-absorption radii deduced from optical-model analysis plotted versus $A^{1/3}$.

does not seem to be so clear, a circumstance which suggests that, of the various strong-absorption radii, $R_{\frac{1}{2}}$ is the most significant. The values of R_{opt} when $a=0.573$ F, together with the strong-absorption radii $R_{\frac{1}{2}}$, $\bar{R}_{\frac{1}{2}}$, and R_σ are plotted in Fig. 9.

We have also attempted to relate strong-absorption radii to optical-model parameters in a less empirical fashion. We may ask,[29] "For what angular momentum l_b does the projectile just surmount the barrier provided by the sum of the Coulomb, centrifugal, and real part of the nuclear potentials?" Again this angular momentum may be used to define an equivalent strong-absorption barrier radius R_b via Eq. (7). The values of R_b corresponding to the best-fit optical potential with $V=-200$ MeV and $a=0.573$ F are 0.07 ± 0.01 F larger than the values of $R_{\frac{1}{2}}$ listed in Table IV. The values of R_b corresponding to the best-fit optical potential with $V=-200$ MeV but with unrestricted values of a are also plotted in Fig. 9. It seems that these values of R_b exceed $R_{\frac{1}{2}}$ by 0.03–0.10 F.

Ford, Hill, Wakano, and Wheeler[30] have noted that, were the potential barrier parabolic in shape, l_b should equal $\bar{L}_{\frac{1}{2}}$ (the angular momentum for which the transmission $1-|\eta_l|^2$ equals $\frac{1}{2}$). Rawitscher[31] has found in an analysis of α scattering from ^{58}Ni with an exponential potential that l_b and $\bar{L}_{\frac{1}{2}}$ are essentially equivalent. In the present analysis, however, R_b is located midway between $R_{\frac{1}{2}}$ and $\bar{R}_{\frac{1}{2}}$. In other words, the calculated transmission at l_b is larger than $\frac{1}{2}$. We think that this is due to the tail of the imaginary potential which

[29] J. S. Blair, Phys. Rev. **108**, 827 (1957).

[30] K. W. Ford, D. L. Hill, M. Wakano, and J. A. Wheeler, Ann. Phys. (N.Y.) **7**, 239 (1959).

[31] G. H. Rawitscher, Nucl. Phys. **83**, 259 (1966).

extends beyond r_b. Indeed, in a model calculation, we reduced the radius and the diffuseness of the imaginary potential just enough to make it negligible beyond r_b. We then found that $l_b=\bar{L}_{\frac{1}{2}}\pm0.01$.

Having introduced the strong-absorption barrier radius R_b, we find it worthwhile to inquire further at what radius r_b is the top of the barrier actually surmounted for a grazing collision, and what is the value $[V(r_b)]$ of the real part of the nuclear potential at this radius? Such a calculation can be carried through numerically for any given potential, but it is often more instructive to work with the simple approximate expressions resulting from the assumption that the potential is purely exponential, with diffuseness parameter a, in the region of interest. One then obtains the relations[29,32]

$$R_b-r_b\approx a[1+\tfrac{3}{2}(a/r_b)]\approx a[1+\tfrac{3}{2}a/(R_b-a)] \quad (12a)$$

and

$$V(r_b)\approx[a/(r_b-2a)][2E-(ZZ'e^2/r_b)]. \quad (12b)$$

[Equation (12a) is actually not quite that given in Refs. 29 and 32 but is an improvement obtained by retaining terms of order a^2.] For ^{58}Ni, where $R_b=$ 7.905 F, we would have from these formulas $r_b\approx7.273$ F and $V(r_b)\approx-6.24$ MeV. (We note that exact evaluation of the Woods-Saxon potential places r_b at 7.243 F, where the value of the potential is -6.52 MeV.) This analysis thus indicates that the magnitude of the real part of the optical potential is relatively small in the highly important region near the top of the barrier.

[We also note that $V(r_b)$ as estimated by Eq. (12b) depends upon the bombarding energy, diffuseness parameter, nuclear charge, and r_b. The dependence on charge and r_b leads to values of $V(r_b)$ which, for fixed E and diffuseness parameter, decrease with increasing mass number, and thus results in values for strong-absorption radii that, on the average, increase faster with $A^{1/3}$ through the Periodic Table[28,33–35] than do the midpoint radii of "best-fit" optical potentials whose depths have been kept constant, a result which has been frequently considered paradoxical.]

The observations of the previous paragraphs may be put in an alternative and often stated form[29,36,37]: Granted that the spherical optical model provides a valid description of the scattering, what is reliably determined in these situations of strong absorption is the real potential in the extreme surface region around that radius which corresponds to a grazing classical trajectory.

As an application of this point of view, we may introduce yet another variety of radius that is particularly appropriate to optical-model analyses: Let us adopt, as a matter of convention, some constant magnitude of the real potential that is of the order of the values at the top of the barrier, and then inquire at what radius this value is attained. The discussion of the preceding paragraph suggests 7 MeV as a reasonable value for the real potential. Accordingly, we would define R_7 through the requirement $V(R_7)=-7$ MeV. The values of R_7, for the best-fit potentials, are also entered into Table II. When, on the other hand, the optical analysis is made with a held fixed at 0.573 F, the values of R_7 will exceed $R_{\rm opt}$ by the constant amount $(3.317)(0.573)=1.90$ F, so that the corresponding plot of R_7 will lie parallel to that of $R_{\rm opt}$ as shown in Fig. 9. Whether we use the best-fit potentials or those with a held fixed at 0.573 F, the values of R_7 are the same to within 0.02 F. The isotopic dependence of the quantity R_7 is clearly much the same as the strong-absorption radii $R_{\rm FC}$, $R_{p\frac{1}{2}}$, $R_{\frac{1}{2}}$, and R_b, already discussed.

Of course, one can suggest alternatively other magnitudes of the real nuclear potential as those most crucial to the scattering process. Thus Jackson and Morgan[36] hold that it is the real nuclear potential at the strong-absorption radius $R_{\frac{1}{2}}$ (which lies approximately a distance a beyond the top of the nuclear barrier) that is the invariant characteristic of elastic scattering analyses at a given bombarding energy and nearly equal values of nuclear charge. Their suggestion is well borne out by the present work. Indeed, our earlier semiempirical observation, that $R_{\frac{1}{2}}$ is approximated by the sum $R_{\rm opt}+4.4a$, may be case in alternative form: The radius at which the real nuclear potential becomes -2.43 MeV (for 42-MeV α particles incident on our range of targets) is within ±0.02 F of the strong-absorption radius $R_{\frac{1}{2}}$ appropriate to the optical-model analysis. This value for the real part of the nuclear

TABLE V. Influence of energy variations on strong-absorption radii.

Nuclide	Mean energy (Lab) (MeV)	$R_{\rm FC}$ (F)	$R_{\frac{1}{2}}'$ (F)	$R_{p\frac{1}{2}}$ (F)
^{40}Ca	41.78	7.281	7.360	7.296
	40.48	7.316	7.410	7.336
	39.03	7.314	7.382	7.348
^{50}Ti	41.92	7.526	7.586	7.542
	40.58	7.546	7.586	7.568
	39.13	7.540	7.601	7.577
^{62}Ni	41.98	7.928	8.001	8.023
	40.45	7.967	8.051	8.053
	39.01	7.959	8.056	8.054

[32] J. S. Blair, in *Lectures in Theoretical Physics VIIIC—Nuclear Structure Physics*, edited by P. D. Kunz, D. A. Lind, and W. E. Britten (University of Colorado Press, Boulder, 1966), p. 343.
[33] D. D. Kerlee, J. S. Blair, and G. W. Farwell, Phys. Rev. **107**, 1343 (1957).
[34] R. H. Venter and W. E. Frahn, Ann. Phys. (N.Y.) **27**, 3 (1964).
[35] M. Rahman, A. H. Kahn, and H. M. Sen Gupta, Nuovo Cimento **L**, B40 (1967).
[36] D. F. Jackson and C. G. Morgan, Phys. Rev. **175**, 1402 (1968).
[37] G. H. Rawitscher, Nucl. Phys. **85**, 337 (1966).

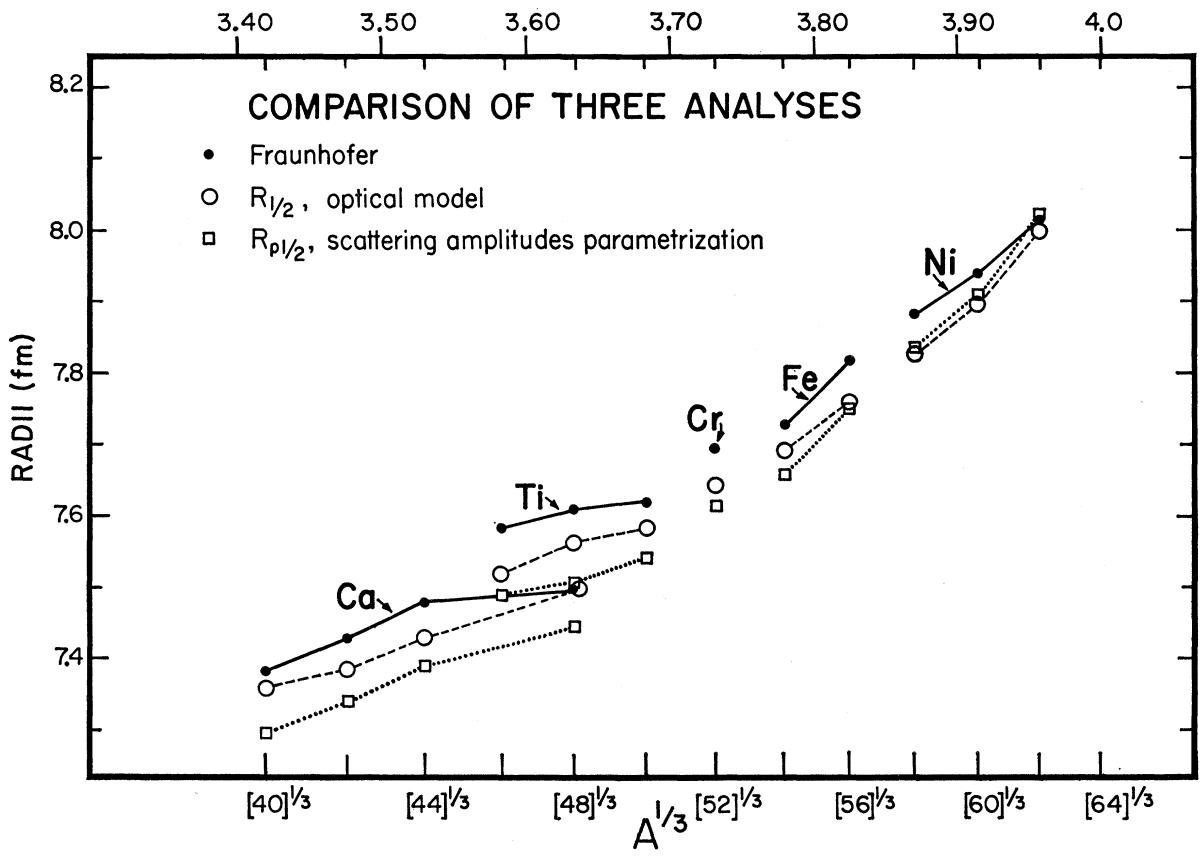

FIG. 10. Comparison of strong-absorption radii deduced from three different theoretical models. The Fraunhofer radius here shown is is for the choice of argument $x=2kR_F \sin(\theta/2)$.

potential is in very close accord with the values found by Jackson and Morgan in an independent analysis of the elastic scattering of 42-MeV α particles from ^{42}Ca.[8]

At the present time, it is not clear to us what will prove to be the very best way of characterizing an optical potential in these situations of strong absorption. Our suggestion of two paragraphs preceding involves the least effort since it does not require the prior determination of $R_{\frac{1}{2}}$, but on the other hand, the recipe of Jackson and Morgan may yield the better invariant. Perhaps we should not belabor these differences since, when the uncertainty in values of a is slight, knowledge of the real part of the potential at $R_{\frac{1}{2}}$ allows us to infer R_7.

D. Energy Dependence

Run IV enabled us to estimate the energy dependence of the strong-absorption radii, operationally defined in the preceding sections. These are listed in Table V. It is reassuring to find that for the three selected isotopes ^{40}Ca, ^{50}Ti, and ^{62}Ni, the differences between values of a particular kind of radius at the three incident energies 42.0, 40.65, and 39.2 MeV do not exceed 0.06 F, the values at the lower energies never being less than those at 42.0 MeV. Indeed, the approximate analysis resulting in Eq. (12) leads us to expect some energy dependence in the strong-absorption radii if there is no change in optical-model parameters. Specifically, the strong-absorption-barrier radius R_b should increase by 0.05 F when the incident energy is dropped from 42.0 to 39.2 MeV, a trend consistent with the values of Table V. However, detailed inspection of the best-fit parameters at the lower energies shows that the observed changes in strong-absorption radii can also be produced by rather small variations in two or more optical parameters. Thus, we cannot argue with any confidence that the small increases in strong-absorption radii as the energy is decreased constitute evidence for energy independence of the potential.

E. Intercomparisons between Models

On the whole there is rather good agreement between the radii of the scattering-amplitudes parametrization and the corresponding radii of the optical model. To illustrate this, we plot in Fig. 10 the radii $R_{\frac{1}{2}}$ and $R_{p\frac{1}{2}}$ as well as the Coulomb-corrected Fraunhofer radius R_{FC} [with $x=2kR_F \sin(\theta/2)$] versus $A^{1/3}$. Similar isotopic trends are exhibited by all three radii although we do note certain systematic deviations. For the Ca isotopes, $R_{\frac{1}{2}}$ is, on the average, larger than $R_{p\frac{1}{2}}$ by

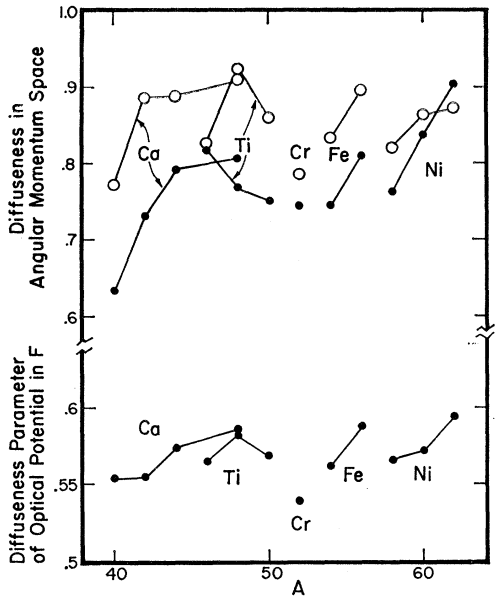

FIG. 11. The diffuseness parameters in angular-momentum space and the diffuseness parameter of the optical potential plotted versus A. In the top portion, the open circles refer to Δ of the scattering amplitudes parametrization while the solid circles refer to δ of the optical-model analysis.

0.05 F. On the other hand, in the Ni isotopes $R_{\frac{1}{2}}$ and $R_{p\frac{1}{2}}$ are essentially equivalent. These radii are straddled by the two varieties of Fraunhofer radii, the variety shown in the figure being closest to $R_{\frac{1}{2}}$ and $R_{p\frac{1}{2}}$ at the upper end of the diagram.

The degree of agreement between the radii deduced from the Fraunhofer analysis and the scattering amplitudes parametrization is not unexpected since analytic approximations[19] to the partial-wave sum for the imaginary part of the scattering-amplitude yield the Fraunhofer amplitude modulated by a damping factor. Similarly, we could have anticipated good agreement between these radii and the strong-absorption radii of the optical-model analysis since it has long been known that the partial-wave amplitudes from optical-model calculations are approximated in situations of strong absorption by the form of parametrization we have adopted.

An additional, and intriguing, correspondence is that the Coulomb-corrected Fraunhofer radii [with the choice of argument $x=2kR\sin(\theta/2)$] do not differ from the strong-absorption-barrier radii R_b by more than 0.05 F. To the extent that these radii may be equated, we are furnished a useful means for estimating the magnitude of the real potential in the extreme surface region without the necessity of carrying out optical-model calculations, simply through inversion of the relation defining R_b. Using the approximate relations mentioned earlier [Eqs. (12)] and making a reasonable estimate for the diffuseness parameter, we can thus estimate $V(r_b)$, and consequently $V(R_{\mathrm{FC}})$, to within 20% from knowledge of R_{FC} alone.

F. Diffuseness

Although our primary attention is directed toward the strong-absorption radii, it is also worthwhile to examine the diffuseness of the partial-wave scattering amplitudes in the transition region between complete and no absorption. In Fig. 11 are plotted Δ and δ, the measures of diffuseness in angular-momentum space for the method of direct parametrization and the optical model, respectively. On the whole, the values of diffuseness for the optical model are less than those for the scattering amplitudes parametrization. However, this difference is due largely to the procedure we followed in fitting the parametrization given by Eq. (10) to the discrete values of $\mathrm{Re}\eta_l$ resulting from the optical-model analysis: Only those partial waves were considered for which $l\geq(L_{\frac{1}{2}}-1)$.

In view of the several obvious cases where these two parameters do not show the same isotopic trends, it is probably hazardous to make any statements about the isotopic dependence of the diffuseness. However, it does seem that the diffuseness of the scattering amplitudes for ^{40}Ca is noticeably less than it is for the other Ca isotopes. But even this conclusion should be greeted with some caution. Inspection of the angular distributions themselves shows that the smaller values for Δ and δ in ^{40}Ca are required primarily to fit the cross sections at our most backward maximum near 50°, which are definitely higher for ^{40}Ca than they are at the corresponding maxima for the other isotopes. Recalling, however, the anomalies found in the ^{40}Ca cross sections of the extreme back angles,[15,17] we speculate that the behavior of our cross sections near 50° may reflect some departure from smooth dependence of the partial-wave amplitudes on l that is outside the framework of our chosen parametrization or optical model rather than an actual diminution in the parameters Δ and δ characterizing smoothly dependent amplitudes.

We have not uncovered any relation between the diffuseness of the transition in angular-momentum space and the diffuseness parameter of the potential that is as simple or trustworthy as those, discussed in Sec. C, relating the optical parameters to strong-absorption radii. We do find as a qualitative rule, within the small range of parameters here studied, that an increase in δ is accompanied by an increase in W/V when a is held fixed, and by an increase in both a and W/V when both are allowed to change. We have included in Fig. 11 a plot of a versus A to illustrate the degree of correlation (or lack thereof) that exists between δ and a. It is worth noting that this observation, correlating increasing δ with increasing a, runs counter to an equation derived by Rawitscher[31] by considering penetration through a real potential barrier.

If the numbers deduced for a are taken at their face value, there does appear to be a trend in the Ca, Fe, and Ni isotopes for the diffuseness parameter of the optical potential to increase with increasing neutron

number. However, this quantity is much less well determined in our experiments than are the strong-absorption radii. Our experience has been that moderately small changes in the experimental data, such as a 4% change in normalization, can result in greatly altered values for the diffuseness parameter a although the same changes lead to no significant alteration in the values of $R_{\frac{1}{2}}$.

IV. DISCUSSION

In the previous sections, we have commented on the consistency in the values of the various kinds of radii we have introduced. Bearing in mind the small differences which were found between the similarly defined radii of the scattering-amplitudes parametrization and the optical model, we now turn to a consideration of the isotopic dependence of these radii.

Inspection of Figs. 5, 9, and 10 leads us to draw the following conclusions:

(1) The strong-absorption radii increase monotonically with $A^{1/3}$ except for those of ^{48}Ca.

(2) On the other hand, the slopes of lines joining corresponding radii of neighboring isotopes are not constant throughout the region. When the slopes $\Delta R/\Delta(A^{1/3})$ are characterized by the parameter r_0, we find between ^{40}Ca and ^{44}Ca that r_0 is in the range 0.6–0.9 F for the radii $R_{\frac{1}{2}}$, $R_{p\frac{1}{2}}$, R_{FC}, and R_{opt} (when a is held fixed at $a=0.573$ F). Similarly, the slopes of lines connecting the corresponding radii of ^{46}Ti and ^{50}Ti are very small, lying between 0.4 and 0.7 F. On the other hand, between ^{58}Ni and ^{62}Ni, we find for radii of the same type that r_0 lies between 1.9 and 2.0 F, and likewise the change in radii for the two Fe isotopes is large. In contrast, the slopes of the lines joining corresponding radii of ^{62}Ni and ^{40}Ca lie between 1.17 and 1.35 F. In view of these trends it is worth recalling that ^{48}Ca has a smaller rms charge radius than ^{40}Ca,[2,6] that ^{46}Ti and ^{50}Ti have essentially equal rms charge radii,[3] and that the rms charge radii[6] of Fe and Ni isotopes increase in a normal fashion with $A^{1/3}$.

The observations of the preceding paragraph may be cast into more pictorial terms. When a straight line is drawn joining the corresponding strong-absorption radii of ^{62}Ni and ^{40}Ca, we see that the radii of the intervening nuclei fall on a bow which lies under the straight line. (It may be objected that too much importance is being attached above to small differences between large numbers. We should like to point out, however, that the quantities most precisely determined in our experiment are the differences in corresponding radii of nuclei belonging to the same run and that the uncertainties in such differences probably do not exceed ± 0.02 F.)

(3) For the radii defined in terms of transmission coefficients or reaction cross sections, a pattern is found similar to that described above. There is a tendency, however, for these radii to increase somewhat more steeply through a given set of isotopes than does $R_{\frac{1}{2}}$ or $R_{p\frac{1}{2}}$. In part, this reflects the isotopic dependence of the diffuseness parameters in angular-momentum space.

(4) For all types of radii, the values for ^{48}Ca appear to be anomalously low when compared to corresponding radii in the neighboring Ti isotopes. Similarly, the increase in going from ^{44}Ca to ^{48}Ca is usually less than the difference in the radii of ^{40}Ca and ^{44}Ca. The result of Bernstein *et al.*,[10] that $[R_{\mathrm{opt}}(^{48}\mathrm{Ca})-R_{\mathrm{opt}}(^{40}\mathrm{Ca}]\cong 0.15$ F when there is no change in surface thickness, is in good agreement with the corresponding differences we observe for the strong absorption radii $R_{\frac{1}{2}}$ and $R_{p\frac{1}{2}}$ and the optical-model midpoint radii (with constant surface diffuseness, $a=0.573$ F).

(5) Igo and Wilkins[38] have reported that the nonelastic cross sections for 40-MeV α particles show a pronounced dip near $Z=28$. Specifically, they state that the reaction cross sections minus the compound elastic cross sections for targets of natural Ti, Fe, and Ni are 1500 ± 37, 1436 ± 42, and 1354 ± 37 mb, respectively. In contrast, we find no indication of a dip in our strong-absorption radii at $Z=28$, nor do we see any strong decrease in the calculated reaction cross sections corresponding to our best fits. The computed optical-model reaction cross sections at 42 MeV for natural abundances of Ti, Fe, and Ni are 1496, 1520, and 1518 mb, respectively. (In obtaining these values, the cross sections of isotopes not studied in our experiment were set equal to those of the next lightest isotope which was studied.) Direct measurements of the reaction cross sections of 24.7α particles[3,l] have also shown no decrease at $Z=28$.

What are the implications of these systematics to the nuclear-matter distributions? According to the most optimistic line of argument, the scattering is described correctly by the spherical optical model and the experiments determine reliably, not just the strong-absorption radii, but, further, the optical potential throughout the surface region. The real part of the optical potential represents some folding operation performed on the matter density, and, consequently, inversion of this folding leads to the matter distribution itself. Presumably, then, the observed isotopic dependence of the strong-absorption radii reflects that of the matter distribution in its rareified tail, the variations being related to obvious differences in shell structure first as the $f_{7/2}$ neutron orbitals are being filled, and later as the $p_{3/2}$ and $f_{5/2}$ neutron orbitals are being occupied.

There are, however, several objections to so sanguine a view, which we now enumerate:

(a) Granted that an optical-model description is appropriate, the spherical model is incomplete in that it does not contain explicitly the coupling of the elastic channel to some other channels known to be strongly

[38] G. Igo and B. Wilkins, Phys. Rev. **131**, 1251 (1963).

[39] A. Budzanowski, K. Grotowski, J. Kuzminski, H. Niewodniczanski, A. Strzalkowski, S. Sykutowski, J. Szmider, and R. Wolski, Nucl. Phys. **A106**, 21 (1968).

excited. Since there are significant variations in the quadrupole and octupole strengths of excited states in the isotopes studied,[8,40–42] it is quite possible that some apparent changes in radii and diffuseness are merely reflections of these variations. The importance of such effects can be estimated by carrying out coupled-channel calculations that do treat explicitly at least some of the extra degrees of freedom of the nuclear system. However, an approximate analytic discussion of the terms in the elastic scattering amplitude that are second order in the collective surface coordinates indicates[43,44] that collective surface coupling increases very slightly the apparent value of the strong-absorption radius, and that the main effect of the coupling is a greater diffuseness in the plot of partial-wave scattering amplitudes versus l, and, consequently, a greater falloff in the envelope to the diffraction oscillations.

To ascertain these effects more quantitatively, we have carried out some coupled-channel calculations with the codes of Wills[45] and Tamura,[46] expanding the complex optical potential through second order in deformation parameters. Three types of calculations were performed: (i) Considering only quadrupole couplings and using the spherical optical-model parameters previously determined for the case $a=0.573$ F, we computed the elastic cross sections and the inelastic cross sections to the first 2^+ level for the various isotopes. The deformation parameters β_2 were chosen to give a fair fit to the inelastic cross sections at prominent maxima. The locations of the minima near 35°, $\theta_{\min}$, were found to decrease by $(0.04°\pm0.03°)$, which is within the experimental uncertainties in the determination of this quantity. (ii) The calculations just described have the defect that the envelope of the maxima in the elastic cross sections now falls off too rapidly with angle. Sample calculations indicate, however, that when the imaginary depth is decreased by amounts necessary to restore the observed falloff, the values of $\theta_{\min}$ are decreased further by less than 0.05^0. (iii) Some calculations which include excitation of both the first 3^- and 2^+ levels suggest that such inclusion will do no more than double the decrease in $\theta_{\min}$ found for case (i). We thus conclude that, were complete channel analyses made of our data, the radius parameters characterizing the extreme surface of the generalized potential would rarely be decreased by amounts larger than their experimental uncertainty ($\sim\pm$ 0.02 F), and that the bowing discussed in Sec. IV B cannot be attributed to the isotopic dependence of the collective transition strengths to the lowest quadrupole and octupole states.

(b) Until such a program is explicitly carried out, it is by no means obvious that reasonable optical potentials for α particles can be generated by folding effective two-body interactions into matter densities inferred from shell-model calculations. However, some recent calculations by Jackson and Morgan,[47] using a Gaussan effective two-body interaction, have given much encouragement that such a program will prove successful.

(c) We should emphasize again that number of quantities given reliably by our experiments is small, and this circumstance limits severely the deductions concerning nuclear structure which one would like to make. The strong absorption radii can be determined with small relative error, but we are faced with much larger uncertainties in our determinations of the diffuseness of the scattering amplitudes or of the diffuseness of the optical potential. This means, assuming the appropriateness of the spherical optical-potential model, that our description of the real potential, even through the surface region, is far from firm. Extrapolation of the potential from the extreme surface region, where the discussion in Sec. III C indicates that it is reasonably well determined, in toward the nuclear interior is subject to many uncertainties, not the least of which is the amplification of uncertainties in the diffuseness parameter.

In conclusion, we warn[29,36] particularly against attaching great significance to one specific best-fit midpoint radius in the optical potential (corresponding either to a discrete or continuous depth-radius ambiguity) and caution that it is yet an act of faith to relate these midpoint potential radii to the corresponding midpoint radii of the matter distribution.

ACKNOWLEDGMENTS

We gratefully express our indebtedness to R. J. Peterson, whose preliminary studies gave impetus to the present work; A. Bernstein, J. Alster, and J. P. Schiffer, whose comments have influenced the design of this experiment and its analysis; D. F. Jackson, for much fruitful discussion concerning the relation between optical potentials and the nuclear matter density; J. Heagney, A. Kolasinski, and W. Q. Sumner for their assistance with experimental problems and the data taking. One of us (B.F.) wishes to acknowledge the warm hospitality of the University of Washington Nuclear Physics Laboratory.

[40] E. P. Lippincott and A. M. Bernstein, Phys. Rev. **163**, 1170 (1967).
[41] A. M. Bernstein, E. P. Lippincott, G. T. Sample, and C. B. Thorne, Nucl. Phys. **115**, 79 (1968).
[42] G. Bruge, J. C. Faivre, H. Faraggi, and A. Bussiere, Nucl. Phys. (to be published).
[43] N. Austern and J. S. Blair, Ann. Phys. (N.Y.) **33**, 15 (1965).
[44] J. S. Blair, in Proceedings of the International Conference on Heavy Ion Physics, Heidelberg, 1969 (to be published).
[45] J. G. Wills, Ph.D. thesis, University of Washington, 1963 (unpublished).
[46] T. Tamura, Rev. Mod. Phys. **37**, 679 (1965).
[47] D. F. Jackson and C. G. Morgan (private communication).